isvr Institute of Sound and Vibration Research

Luminescence from Hydrodynamic Cavitation: Method and Preliminary Analysis

T.G. Leighton, M. Farhat, J.E. Field and F. Avellan

ISVR Technical Report No 294

June 2001

University of Southampton

SCIENTIFIC PUBLICATIONS BY THE ISVR

Technical Reports are published to promote timely dissemination of research results by ISVR personnel. This medium permits more detailed presentation than is usually acceptable for scientific journals. Responsibility for both the content and any opinions expressed rests entirely with the author(s).

Technical Memoranda are produced to enable the early or preliminary release of information by ISVR personnel where such release is deemed to the appropriate. Information contained in these memoranda may be incomplete, or form part of a continuing programme; this should be borne in mind when using or quoting from these documents.

Contract Reports are produced to record the results of scientific work carried out for sponsors, under contract. The ISVR treats these reports as confidential to sponsors and does not make them available for general circulation. Individual sponsors may, however, authorize subsequent release of the material.

UNIVERSITY OF SOUTHAMPTON

INSTITUTE OF SOUND AND VIBRATION RESEARCH

FLUID DYNAMICS AND ACOUSTICS GROUP

Luminescence from Hydrodynamic Cavitation: Method and Preliminary Analysis

by

T G Leighton°†, M Farhat*, J E Field°, F Avellan*

° Cavendish Laboratory, Madingley Road, Cambridge CB3 0HE, UK

* Institut de Machines Hydrauliques et de Mécanique des Fluides,
École Polytechnique Fédérale de Lausanne (EPFL), 33, Av. de Cour, Lausanne, Switzerland

† Now at Institute of Sound and Vibration Research (ISVR),
University of Southampton SO17 1BJ, UK

ISVR Technical Report No. 294

June 2001

Authorized for issue by
Professor C L Morfey, Group Chairman

ACKNOWLEDGEMENTS

JEF and TGL thank Professor F Avellan and EPF Lausanne for the opportunity to bring the Cambridge photon detectors to perform an experiment on the IMHEF cavitation tunnel. The research was performed during a series of study leave visits and EPFL, The Royal Society (London) and the Royal Academy of Engineering (London) are thanked for their support.

CONTENTS

FIGURE CAPTIONS

Figure 1
Two-dimensional cavity, diameter 3 mm, collapsed by a shock wave travelling left to right. The rear surface involutes to produce a jet, J, of *ca.* 400 m s^{-1}. Interframe time 0.96 μs. (Dear *et al.*, 1988).

Figure 2
a) A 3-mm diameter cavity before collapse, and (b) its time integrated luminescence. The shock moved left to right. The luminescence is concentrated in the lobes on either side of the jet. (Dear *et al.*, 1988)

Figure 3
Top view of leading edge cavitation on a NACA 009 2-D hydrofoil of 100 mm chord length. The flow is from the left. $C_{ref} = 30$ m/s, $\alpha = 3.5°, \sigma = 0.9$.

Figure 4
Generation mechanism for transient U-shaped vortices in a leading edge cavitation flow. Aligned top and side view are shown. The arrows denote the directions of vortex rotation and movement away from the hydrofont. (After Dupont, 1993).

Figure 5
Illustration of (a) stable and (b) unstable cavitation. The flow is from the left.

Figure 6
A schematic of the *IMHEF* high-speed cavitation tunnel.

Figure 7
Experimental hydrofoil (NACA 009). The chord length is 100 mm.

Figure 8
A schematic of the apparatus used to generate and detect sonoluminescence.

Figure 9
(a) The voltage pulse emitted by the discriminator which is the trigger for the LeCroy oscilloscope; and (b) the corresponding output of the LeCroy when triggered by (a). Both traces have a total length of 2 μs.

Figure 10
Operation of the Signal Averager.

Figure 11
The time series of photon arrivals, as determined from the output of the LeCroy; Data Acquisition System 2 in Figure 8. Each photon arrival is indicated by a voltage pulse of standardised amplitude, 0.1V and duration 1 μs. The output is shown for three values of the flow speed, C_{ref}, of *ca.* 20, 25, and 30 m/s, and cavitation index , σ, of *ca.* 0.8, 0.75, and 0.7. The angle of attack, α, is 2.5°. The precise values are (a) 19.97 m/s, 0.81; (b) 24.89 m/s, 0.80; (c) 29.91 m/s, 0.80; (d) 19.93 m/s, 0.74, (e) 24.86 m/s, 0.74; (f) 29.85 m/s, 0.75, (g) 20.28 m/s, 0.62; (h) 24.76 m/s, 0.70; (i) 29.73 m/s, 0.71. The sampling frequency was 2

Msamples/s. In (h) and (i), where the photon counts are greatest, the count is terminated at *ca.* 190 ms and 150 ms respectively owing to complete filling of the acquisition memory.

Figure 12
Number of windows versus number of photons in one window for different values of velocity C_{ref}, constant $\alpha = 4°$ and $\sigma \sim 1.1$.

Figure 13
Number of windows versus number of photons in one window for different values of σ, constant $\alpha = 4°$ and $C_{ref} \sim 30$ m s^{-1}.

Figure 14
Selected window occupancy histograms for increasing flow speed for $\alpha = 4°$ and $\sigma \sim 1.1$. The "window index" is the window with this number of photons. Note there is always a zero occupancy count, not illustrated. In the presence of cavitation there is a second peak, as illustrated, which has an increased occupancy at higher flow speed.

Figure 15
Total number of detected photons as a function of flow speed for $\alpha = 4°$ and $\sigma \sim 1.1$.

Figure 16
Total number of detected photons as a function of cavitation index for $\alpha = 4°$ and $C_{ref} \sim 30$ m/s.

Figure 17
Expected window occupancy histogram for unstructured signal.

Figure 18
Expected window occupancy histogram for signal containing both structure and noise.

ABSTRACT

This report describes a photon-counting study of the cavitation luminescence produced by flow over a hydrofoil. The object was to obtain *quantitative* data on the number of photons emitted for various flow conditions and to study the link between the light output and the potential for cavitation damage. The flow experiments were performed in a cavitation tunnel capable of achieving flow velocities of up to *ca.* 50 m s^{-1} in the test sections. The experimental hydrofoil was a NACA 009 blade. Parameters varied were the flow velocity, the incident angle of the hydrofoil and the cavitation index. The results show that significant photon counts are recorded when leading edge cavitation takes place and U-shaped vortices (cavities) shed from the main cavity. The photon count increases dramatically as the flow velocity increases or the cavitation index is reduced. Departure from a Poisson distribution in the arrival times of photons at the detector may be related to the way vortices shed from the main cavity. Finally, there is a clear correlation between light output and the conditions which could cause cavitation damage.

1 INTRODUCTION

The development of leading edge cavitation on a hydrofoil is a potentially dangerous erosion situation. This type of cavitation is usually encountered on hydraulic runners and is characterised by the formation of a vapour cavity attached to the leading edge of the blades. This main cavity sheds vapour cavities, entrained within vortices in the liquid. These transient features are convected by the flow and collapse violently in the pressure recovery region. The resulting overpressure may reach up to 2 GPa (Avellan and Farhat 1988). Cavitation erosion is caused by these repeated collapses. Such cavitation also gives rise to a number of other effects, notably acoustic emissions, which include pressure waves generated when the cavities collapse. The emission can be generated from rebound shocks or through liquid jet impact if the bubble involutes during collapse. In addition to these, cavitation can also cause luminescent emissions. Although, as Walton and Reynolds (1984) point out, the term 'cavitation luminescence' would be a better description for emissions that result from the cavitation generated by hydrodynamic flow, liquid impact, laser and spark discharge, and the collapse of vacuums, colloquially these are often termed 'sonoluminescence'. This inappropriate nomenclature arose from majority use of acoustics to generate the cavitation in the early decades (Marinesco and Trillat, 1933; Jarman, 1960; Knapp *et al.*, 1970). Current debate on the commonality of the sources of the various luminescences calls this practice in question (Barber *et al.* 1997; Blake *et al.*, 1999; Leighton *et al.* 2000; Hammer and Frommhold 2001).

Compared with the prevalence of acoustic systems, there are few studies on the cavitation luminescence generated by hydrodynamic flow (Peterson, 1966, 1967; van der Meulen 1983a, b, 1986 a, b). van der Meulen used a high-speed flow tunnel with a NACA 16-022 hydrofoil set at various angles. By changing the angle of attack on the blade, α, and the

velocity, he produced four regimes of flow which he termed (i) bubble, (ii) sheet, (iii) sheet-cloud, and (iv) vortex-cloud cavitation. These regimes were studied photographically and both noise and luminescence measurements made. For the luminescence experiments, xenon gas was added to the deaerated water; this enhanced the luminescence. The luminescence from the flow passed through a PMMA (polymethylmethacrylate) window then, by way of a mirror and slit, into a RCA PF 1011 photomulitplier. Relative intensity measurements were taken, with no attempt made to measure the absolute light intensity (i.e. number of photons involved).

The bubble cavitation, $\alpha = 2°$, was anomalous in that the intensity *decreased* with increasing velocity (range 10 to 20 m s^{-1}). However, all the other types of flow gave positive velocity exponents, m. In the noise measurements, the velocity exponents, n, were always positive and considering the complexity of the measurements the agreement between n and m for the flow types (ii) and (iv) is important. van der Meulen's data are summarised in Table 1. van der Meulen concluded that his research had established a useful link between erosion, noise generation and luminescence.

As stated earlier, the impact of the jets formed by bubble involution can cause both erosion and acoustic emission and an association between such jetting and luminescent emission is demonstrated in the following two figures taken from Dear and Field (1988) and Dear *et al.* (1988). Figure 1 shows the collapse of a circular two-dimensional cavity formed in a gel by a shock of strength 0.26 GPa. The shock can be seen by encircling the cavity in frame 1. The rear surface of the cavity begins to involute to form a jet in frame 5. The jet crosses the cavity and the gas is compressed into two lobes. Other work (Bourne and Field, 1992) has shown

that these lobe regions progress as a pair of vortices which travel downstream after the shock. In a three-dimensional cavity, the gas would be compressed into an annulus.

Figure 2 shows a single 3-mm diameter cavity collapsed under similar conditions to those in Figure 1 but this time viewed through an image intensifier. The image shows the time-integrated luminescence from the collapsed cavity. A small amount of background lighting has been added to reveal the shape of the uncollapsed cavity. There is a bright spot on the side of the cavity where the shock first interacts, but this did not appear in all sequences and is probably and artefact caused by an imperfection in the gel surface. It is clear that most light is produced from the two lobe-shaped regions of trapped gas on either side of the jet. These conform to the shape of the cavity wall during the later stages of collapse (see frame 10 of Figure 1).

Measurements of the volume of gas luminescing show that luminescence takes place when the gas volume has been compressed to less than 10% of its initial volume. The luminescence shows a definite structure with some brighter regions, however, which indicates inhomogeneous conditions. Such inhomogeneities have now been predicted by Ball *et al.* (2000). Clearly, therefore, cavity collapses of sufficient energy to create hot spots and erosion may be associated with luminescence, even though the detailed mechanisms causing luminescence need further research.

Cavitation luminescence is often very faint, being at the detector of the order of a few hundred photons per square centimetre per second, with certain exceptions under very specific conditions (Gaitan *et al.*, 1992; Barber *et al.*, 1992). Sensitive light detection equipment is therefore usually required to observe it and the present study employs

photomultiplication. Photomultiplication allows time resolution of the phenomenon even though individual photon pulses do not exceed nanosecond order. Once resolved, such pulses can be counted to quantify the light output, and this was used to determine the relationship between the cavitation luminescence and the upstream velocity, C_{ref}, and cavitation index, σ, in the tunnel. However, the ability to take temporal measurement of the emission was important, since the second aim was to investigate the luminescence for the presence of low frequency structure.

Hydrodynamic cavitation being a somewhat imprecise phenomenon, it is necessary to take many seconds of data to obtain the required statistical validity for any measurement of these low frequencies. Single photon events are, however, short-lived, and so the electronic signal pulses used in photon counting are of nanosecond duration. Few systems can sample at frequencies of 10^9 Hz for several seconds. Care had to be taken (see Section 4) that the sampling frequencies of the detectors were always adequate for the length of pulse at the input, since in such experiments the failure to record some events due to inadequate sampling is often not readily apparent in the results. For this reason, the digital signal was converted to standard pulses at each stage.

2 LEADING EDGE CAVITATION

The generation of transient cavities in leading edge cavitation flow has been widely investigated. Figure 3 shows a top view of leading edge cavitation occurring on a 2-D hydrofoil in the IMHEF high-speed cavitation tunnel for an incidence angle of 4° and an upstream velocity of 30 m/s.

Dupont (1993) investigated the flow field downstream of the main cavity with laser Doppler anemometry and observed an intense shear stress in the vicinity of the main cavity interface. The interaction of the resulting vorticity lines with the Kelvin-Helmholtz instabilities leads to the formation of U-shaped vortices as illustrated in Figure 3. These vapour cavities are convected by the mean flow to the pressure recovery region where they collapse. Figure 4 shows schematically the generation and convection mechanisms for the transient cavities.

Farhat *et al.* (1993) and Farhat (1994) investigated the shedding process of the transient cavities in leading edge cavitation flow by measuring the pressure fluctuations induced downstream of the main cavity. They showed that increases of the incidence angle, the upstream velocity or the cavity length promote instabilities in the main cavity behaviour which strongly influences the shedding process. Figure 5 illustrates the stable and unstable regimes of the main cavity. These photographs were obtained during studies of flow over a 2-D hydrofoil in the IMHEF high-speed cavitation tunnel.

In the stable regime, the size of transient cavities as well as the amplitude of the main cavity fluctuations are small when compared to the main cavity length, and the shedding process is found to be intermittent. When the main cavity is in the unstable regime, the size of transient cavities as well as the amplitude of the main cavity pulsation are of the same order as the main cavity length. In this case, the shedding process is controlled by a Strouhal-type law. The Strouhal number is defined by

$$S = \frac{f_s l_c}{C_{ref}} \tag{1}$$

where f_s denotes the shedding frequency of the transient cavities, l_c is the main cavity length and C_{ref} is the upstream velocity. The Strouhal number depends on the incidence angle and was found to lie between 0.2 and 0.3 for incidence angles ranging from 2° to 5°.

3 EXPERIMENT

3.1 The high-speed cavitation tunnel

The experiments were carried out in the IMHEF high-speed cavitation tunnel (Avellan *et al.*, 1987) and shown schematically in Figure 6. The dimensions of the test are $0.15 \times 0.15 \times 0.75\,\mathrm{m}^3$. A maximum velocity of 50 m/s can be reached at the inlet of the test section. The experimental hydrofoil was a NACA 009 truncated at 90% of its chord length (see Figure 7). The hydrofoil is 100 mm long and 150 mm wide. Its maximum thickness is 10 mm. The operating parameters for the cavitation tunnel which were controlled were the upstream velocity at the inlet of the test section C_{ref}, the incidence angle of the hydrofoil, α, and the cavitation index, σ. The dimensionless cavitation index is related to the pressure at the inlet of the test section, p_{ref}, and is defined by

$$\sigma = \frac{p_{ref} - p_v}{\frac{1}{2}\rho C_{ref}^2} \tag{2}$$

where p_v denotes the vapour pressure and ρ is the liquid density.

3.2 Experimental procedure

The object of the current experiment is to quantify the cavitation luminescence from flow in a cavitation tunnel through photon counting, and to determine the dependence of the emission upon the flow parameters. Analysis of the signals was used to investigate the presence of low frequency structure within the emission. To do this, the major problem that

had to be overcome was the collection of sufficient data to detect frequencies of order 100 Hz when the individual photon events were of nanosecond order.

Figure 8 shows the apparatus used to generate and detect cavitation luminescence . The blade, a NACA 009 hydrofoil, was mounted in the test section of the high-speed cavitation tunnel (Figure 6). The 12.4 mm diameter photocathode was mounted 16 cm above the blade (Figure 8), presenting an acceptance solid angle of 3.75×10^{-4} steradians, so that the photon counts obtained represent approximately 0.0375% of the total luminescence emitted (assuming, to first order, spherical symmetry in the emission).

As a system for measuring low levels of light, photon-counting has three advantages over more conventional techniques such as DC current measurement. First, the long-term gain stability is better, the system gain being relatively insensitive to any fluctuations in the high voltage of the detector. Second, the signal-to-noise ratio is optimised. Third, drifts in the zero offset output (a function of temperature) or DC leakage from the photomultiplier are unable to affect the result. The digital nature of the output is suitable for processing, which in this experiment involved measurement of temporal differences between pulses, and so is sensitive to the presence of noise. The presence of noise photons in the 'quiet' interval between signal photons could contribute spurious high-frequency data. It was essential, therefore, to maintain a high signal-to-noise ratio, to take data over a long period and to discriminate pulses, as detailed below.

The use of a lower threshold on its own to remove noise is not appropriate. Whilst this would eliminate the low amplitude pulses which arise mainly from two sources (spontaneous secondary emission within the photomultiplier, and thermally excited electron emission from

the photocathode), it would not screen out the classes of noise that occur within photomultipliers which have amplitudes greater than the amplitude of pulses resulting from true photon detection. This high-amplitude noise can be due to radioactivity in the proximity of the photomultiplier, or to the Cherenkov photon emissions caused by cosmic ray passage, or by positive ion feedback (where gas molecules within the imperfect vacuum of the photomultiplier becomes ionised by the electric field, and cause high energy pulses). To eliminate these noise sources, it is necessary to include in addition an upper threshold in addition to the lower one. The detection of true photons should result in a pulse of energy intermediate between these two thresholds. Noise pulses should ideally lie outside these thresholds. By careful choice of a fast photomultiplier which in addition emits photon-related pulses within a narrow and well-defined energy range, it is possible to reject both high and low-amplitude noise pulses by the use of a discriminator.

The signal processing and the three possible data acquisition systems are show in Figure 8. The output of the EMI 9789B photomultiplier, supplied at 1150 V, is preamplified and the processed by and EG and G Brookdeal 5C14 Pulse Height Discriminator (part of the Brookdeal 5C1 photon counting system; labelled "Data Acquisition System 1" in Figure 8), which had been given a threshold window appropriate to the photomultiplier used in order to achieve photon-counting. On receiving from the photomultiplier an electric pulse acceptable to the discriminator window, and which was therefore taken to represent a photon signal rather than noise, the discriminator emitted a standard pulse of width of order 10 ns. This pulse was then extended to one of order 1 μs by customising the trigger facility of the LeCroy 9400 oscilloscope (Figure 9). In response to such a triggering event, the LeCroy emits a TTL pulse that may be detected by another instrument. The LeCroy will trigger on all photon pulses except when, in response to being triggered, internal data recording gives the

system a dead time of 200 μs, which determines the limit on detection of closely-spaced pulses. If two or more photons arrive at a spacing of less than 200 μs, only the first is counted. How this affects Figures 12-14, and the subsequent calculation is discussed in Section 6.3.

The output from the oscilloscope is acquired using a LeCroy 6810 waveform digitiser at 2 MHz sampling frequency to give the time series of photon arrivals (Data Acquisition System 2, in Figure 8). Though suitable for providing a visual representation of the photo emissions, a limitation of this system was its inability to handle data sets larger than 250 photons. Further, the memory depth of the 6810 digitiser limits the record length to 256 ms. Therefore, the statistical analysis of the emissions to detect the presence or absence or low-frequency structure output of the oscilloscope was acquired by a Nicolet 370 Signal Averager (Data Acquisition System 3, in Figure 8).

The time series data was divided in the Signal Averager into 20 ms windows, with approximately 1 ms dead time between windows. Analysis by this system produced histograms of window occupation. Each window was classified by how many photons occurred within it, and this classification was employed to determine whether the time series data exhibited low frequency structure. For example, if no photons were found within a given window, the accumulated count for the class of windows having zero-occupancy count was incremented by one (Figure 10). In each case a total of 10,000 windows were examined.

After acquisition, the Signal Averager stored the window occupancy data in an internal memory. This data could then be transferred to the controlling computer HP 382 (HP 18) by a GBIB line. The HP 382 computer is the controlling unit of the whole measurement,

controlling both branches of the acquisition, i.e. photon counting and measurement of the flow parameters in the test section. For practical reasons, the flow parameters are measured and stocked in another computer, a PC-UNIX, from which the data can be transferred by ETHERNET.

The duration of the acquisition was 10,000 windows, which corresponds to 210 s in which photons can be detected, and 20 s of "dead time" during which they cannot. Integration of the window occupancy data enabled the total photon output in the acquisition period to be calculated as a function of tunnel parameters (upstream flow speed, C_{ref}, incidence angle, α, cavitation number, σ). Analysis of the form of the occupancy graphs enabled limits to be set on the lowest possible value of the high frequency structure, and the highest possible value of the low-frequency structure, associated with the luminescence.

4 RESULTS

Figure 11 shows the time series data for cavitation at flow speed of approximately 20, 25 and 30 m/s for $\sigma \sim 0.8$ to ~ 0.7 and $\alpha = 2.5°$. The data are summarised in Table 2. Clearly, the number of counts increases with increasing velocity C_{ref} and decreasing σ.

Figures 12 and 13 show individual histograms showing, on the ordinate, the number of windows in the whole 210 s sequence which have the number of photons per window that is indicated on the abscissa. Figures 12 (a) to (f) show a sequence of six histograms, for increasing flow velocities and approximately constant σ. Figure 13 shows a similar sequence, for decreasing σ and approximately constant flow velocity.

In each case, there is a large count for windows containing no photons, then a broad peak for windows of a higher occupancy. The "noise" histograms, produced for conditions of no cavitation, are shown in Figure 13 (a).

These histograms can be used to determine the photon count under these conditions. By multiplying the ordinate and abscissas from Figures 12 and 13, the total number of photons which occur in windows of a given occupancy (window index) can be found. Such a series of histograms is generated in Figure 14 (a) to (c). From the data in Figure 12, integration of these curves gives the total number of photons detected in the 3.75×10^{-4} steradian solid angle during the 210 s detection time. The variation of output against flow velocity is shown in Figure 15 (obtained by integration of 14); and as a function of σ in Figure 16 (from the data in Figure 13).

5 DISCUSSION

The photon count, taken into a solid angle comprising 0.0375% of the global space, is seen to increase with increasing flow velocity and below $\sigma\sim$ 1.5 with decreasing cavitation index (Figures 15 and 16). Both trends, in C_{ref} and σ, are indicative of increasing cavitation intensity. Former measurements of the cavitation erosion, the induced vibrations and fluid-borne noise show similar trends (Farhat 1994). At the highest level of cavitation, the increase in photon count with increasing C_{ref} does not continue at so great a rate, the fall-off occurring at about $C_{ref}\sim$ 25 m/s, and indeed ceases to increase significantly with decreasing cavitation index below $\sigma\sim$ 1.2. When the cavitation index is decreased, the main cavity closure, from which the transient vortices are generated, moves toward the trailing edge. Furthermore, the cavity dynamics are known to be highly influenced by the flow velocity and the cavitation

index for a fixed incidence angle. For a given cavity length, an increase of the flow velocity may promote strong instabilities which lead to substantial increase of the main volume of the transient cavities. Such instabilities may also be promoted by an increase of the cavity length at a fixed flow velocity. Therefore, the collapse location of the transient cavities moves toward the trailing edge of the blade and may be beyond the field of view of the photomultiplier.

The occupancy histograms indicate low-frequency structure in the luminescence. If the time of arrival of photons were random, then with a small window one would expect the highest occurrence close to zero-occupancy tending to decrease as the number of photons occupying that window increases. Therefore with sufficiently large data sets one would expect randomly spaced (unstructured) photon arrivals to give a histogram of the form illustrated in Figure 17.

However, if there was low frequency structure in the time-series data, windows of higher-than-average (mean) occupancy would occur, separated by regions having occupancy lower than the mean. This would give rise to a 2-peak structure, and if the photon burst were particularly concentrated one would expect the lower window to occur for zero occupancy, giving rise to histograms of the form illustrated in Figure 18.

The noise histograms in Figure 13 (a) are indicative of unstructured arrivals, of the form indicated in Figure 17. However, all the histograms representing cases where cavitation occurred display the two-peak structure of Figure 18, indicating the low-frequency structure in the time-series data.

The data management of nanosecond photon pulses does not in the present arrangement allow measurement of the low-frequency envelope of their time series of arrivals. However, it is possible to extract limits of the minimum value of the high frequency, as well as the maximum value of the low-frequency envelope, which characterises the photon bursts.

5.1 *Limits of the low frequency structure*

The value of the low frequency depends on the organisation of the windows of high-occupancy. Assume to a first approximation that the data set contains only windows which are either empty, or are well-populated to a similar extent. If, in a given data set, all the highly-occupied windows occurred in a single cluster, there would be no period to the bursts. The only statement that can be made is that any low-frequency structure associated with this data envelope would have a period greater than the duration of the experiment (210 s) and therefore a frequency less than $\frac{1}{210}$ Hz. At the other extreme, a high value for this low frequency would occur if the highly-occupied windows occurred singly and evenly spaced. If the windows are evenly spaced, any grouping characteristic between these two limits would give a lower frequency than this. Therefore, this estimates the maximum value for the low-frequency component could take if it is assumed that the window-groups repeat at a single frequency (i.e. are evenly spaced).

In practice there is a range of occupancy values clustered about the mode. The highest value that the low frequency can take is found through finding the number of well-occupied windows through integration of the relevant modal peak of curves of the type shown in Figure 12, and assuming that this number of windows is evenly distributed and not adjacent throughout the time series data.

The results of the calculations are shown in Table 3 for the data relating to constant σ and varying C_{ref} (Figures 12, 14 and 15). Estimates of the number of highly-occupied windows (column (iii)) are obtained by dividing the total photon count (column (i), as shown in Figure 15) by the modal occupancy (column (ii) taken from the high-occupancy peak of data of the type shown in Figure 12 or, equivalently, Figure 14). The estimate of the highest value of the low frequency is therefore obtained by dividing the modal number of highly-occupied windows (column (iii)) by the length of the experiment (210 s). This is shown in column (iv).

Similar values can be obtained for the variation of σ at constant C_{ref} (Table 4).

5.2 *Limits of the high frequency structure*

If the photons within the burst are assumed to be evenly spaced, the minimum value of the high frequency which characterises their emission would simply be the modal occupancy (as given by the curves of the type shown in Figure 13) divided by the window duration (20 ms). Standard error can be associated with each frequency, found from the width of the peaks in Figure 13. These are shown in column (v) of Tables 3 and 4, and are found by dividing the values in column (ii) by 20 ms.

5.3 *Possibility and effect of undercounting*

With any finite dead-time of 200 μs, a window occupancy of greater than 100 cannot be recorded in Figures 12 and 13. However, the more subtle effect of undercounting becomes more likely the greater the occupancy, leading to underestimates of both the total photon

count (Figures 14, 15 and 16) and possibility in the modal occupancy (Figures 12, 13 and 14). The likelihood of the effect on the frequency estimates in Tables 3 and 4 can be assessed. Confidence is justified in rows 1-3 of Table 3 (C_{ref} =18.3, 20.0 and 22.4 m/s), and row 7 if Table 4 ($\sigma = 1.5$), where the modal occupancy is less than 50 photons per 20 ms window (averaging 400 μs between photons), and the effect of under counting is likely to be small. In these rows only is the estimate of the minimum value of the high frequency less than the 2500 Hz Nyquist frequency. As one moves further down Table 3, or up Table 4, the possibility increases that both the total number of photons (col. (i)) and the modal occupancy (col. (ii)) may include an element of undercounting, and so are underestimates. Such would lead to col. (v), the estimate of the minimum value of the high frequency, being an *overestimate*: therefore, the error is on the side of caution. However, the direction of the error in the estimates in rows 4-8 in col. (iv) cannot readily be assessed.

6 CONCLUSIONS

The present research has used photon counting to detect luminescence during flow over a blade in a high-speed cavitation tunnel. Earlier research by Dupont (1993) and Farhat, *et al.*, (1993) and Farhat (1994) has recorded and described the build-up of a main cavity and the conditions under which U-shaped vortices (cavities) shed from the main cavity. The conditions under which these cavities collapse and cause erosion are well-established.

The key result of the present research is that significant photon counts are recorded when the cavities collapse transiently with the potential to cause erosion. The photon count increases dramatically as the velocity C_{ref} is further increased (see, for example, Figure 15) or σ reduced (see Figure 16). Eventually the photon count reaches a plateau. This may be due to

the increased bubble cloud obscuring the source of luminescence or simply the collapse sites moving to a position partly out of the field of view of the photomultiplier.

The luminescence is not uniformly produced with time and this suggests that it may be possible to use the photon counting to monitor the frequency of transient collapse events.

The frequency of transient collapse events is not necessarily related to the shedding frequency f_s in a simple way. As noted in Section 6.3, the number of vortices which shed from the main cavity per second may be higher than f_s since they may shed from multiple points from the rear of the main cavity. Alternatively, if not all of the vortices collapsed transiently (i.e. rapidly), then the frequency of transient events could be less than f_s.

It is possible to make estimates (admittedly crude) of the highest value of the low frequencies and the minimum value of high frequencies from our photon counting and data are given in Tables 3 and 4.

The minimum value of the high frequencies (column (v)) in Table 3 and 4 increases with velocity C_{ref} and gives values approximately an order of magnitude greater than the f_s estimated from equation (1) (assuming an idealised 2-D process). This would suggest that vortices shed from about 15 points along the rear of the main cavity at $C_{ref} = 20$ m s^{-1} and from about 20 points $C_{ref} = 30$ m s^{-1}. This is physically reasonable (Dupont 1993).

In future research, it would be interesting to have a focused system which collected photons from specific regions. This would allow more detailed research on the shedding and transient collapse processes.

Finally, the correlation of luminescence with the onset of transient collapse and cavitation damage provides a potentially useful technique for detecting when blades on a turbine are likely to be eroded.

REFERENCES

Avellan F and Farhat M, 1988. "Shock Pressure Generated by Cavitation Vortex Collapse", *Proc. of Int. Symposium on Cavitation Noise and Erosion in Fluid System*, ASME Winter Annual Meeting, San Francisco (USA), FED-Vol. **88**, *pp.* 119-125.

Avellan F, Henry P and Rhyming I L, 1987. "A new high speed tunnel for cavitation studies in hydraulic machinery", ASME Symposium on "Cavitation research facilities and techniques", Boston, USA, **57**, 49-60.

Ball G J, Howell B, Leighton T G and Schofield M, 2000. "Shock-induced collapse of a cylindrical air cavity in water: a Free-Lagrange simulation", *Shock Waves*, **10**, 265-276.

Barber B P, Hiller R A, Arisaka K, Fetterman H and Putterman S, 1992. "Resolving the picosecond characteristics of synchronous sonoluminescence", *J. Acoust. Soc. Am.*, **91**, 3061-3063.

Barker B P, Hiller R A, Lofstedt R, Putterman S J and Weninger K R, 1997. "Defining the unknowns of sonoluminescence", *Phys. Reports – Rev. Section Phys. Lett.*, **281**, 66-143.

Blake J R, 1999 (Ed. Soc. Land Discussion). "Acoustic cavitation and sonoluminescence", *Phil. Trans. R. Soc. Lond. A* **357**, 199-369.

Bourne N K and Field J E, 1992. "Shock-induced collapse of single cavities in liquids", *J. Fluid Mech.* **244**, 225-240.

Dear, J P and Field, J E, 1988. "A study of the collapse of arrays of cavities", *J. Fluid Mech.* **190**, 409-425.

Dear J P, Field J E and Walton A J, 1988. "Gas compression and jet formation in cavities collapsed by a shock wave", *Nature*, **332**, 505-508.

Dupont P, 1993. "Etude de la Dynamique d'un Poche de Cavitation Partielle en Vue de la Prédiction de l'Erosion dans les Turbomachines Hydrauliques", PhD thesis No 931, EPFL, Switzerland.

Farhat M, 1994. "Contribution á l'Etude de l'Erosion de Cavitation: Mécanismes Hydrodynamique et Prédiction", PhD Thesis No 1273, EPFL, Lausanne, Switzerland.

Farhat M, Pereira F, Avellan F, 1993. "Cavitation Erosion Power as a Scaling Factor for Cavitation Erosion in Hydraulic Machines", *Proc. of the 3rd Int. Symposium on Cavitation Noise and Erosion*, ASME, New Orleans (USA), Fed-Vol. **176**, pp. 95–104.

Gaitan D F, Crum L A, Church C C, Roy R A, 1992. "An experimental investigation of acoustic cavitation and sonoluminescence from a single bubble", *J. Acoust. Soc. Am.*, **91**, 3166-3183.

Hammer D and Frommhold L, 2001. "Sonoluminescence: How bubbles glow", *J. Modern Optics*, **48**, 239-277.

Jarman P, 1960. "Sonoluminescence: a discussion', *J. Acoust. Soc. Am.*, **32**, 1459-1462.

Knapp R T, Daily J W and Hammett F G, 1970. *Cavitation*, McGraw-Hill.

Leighton T G, 1993. *The Acoustic Bubble*, Academic Press, London.

Leighton T G, Cox B T and Phelps A D, 2000. "The Rayleigh-like collapse of a conical bubble", *Journal of the Acoustical Society of America*, **107**, 130-142.

Marinesco M and Trillat J J, 1933. "Action des ultrasons sur les plaques photographiques", *Compt. rend. Acad. Sci.* Paris, **196**, 858-860.

Meulen van der J H J, 1983a. "The use of luminescence as a measure of hydrodynamic cavitation activity", *ASME Cavitation and Multiphase Flow Forum*, Houston, 51-53.

Meulen van der J H J, 1983b. "A study of the relationship between type of cavitation erosion and luminescence", *Proc. 2nd Int. Conf. on Cavitation*, Edinburgh, 13-19.

Meulen van der J H J, 1986 a. "On correlating erosion and luminescence from cavitation on a hydrofoil", *Int. Symp. on Propellers and Cavitation*, Edinburgh, 13-19.

Meulen van der J H J, 1986 b. "The relation between noise and luminescence from cavitation on a hydrofoil" *Joint ACSE/ASME Conf. on Cavitation in Hydraulic Structures and Turbomachinery*, Albuquerque, USA, Vol. 25, 149-159.

Peterson F B, 1966. "Light emission from hydrodynamic cavitation", PhD Thesis, Northwestern University, USA.

Peterson F B, 1967. "Monitoring hydrodynamic cavitation light emission as a means to study cavitation phenomena", *Proc. Symp. on Testing techniques in ship cavitation research,* **2**, Trondheim, Norway, pp 3-17.

Walton A J and Reynolds G T, 1984. "Sonoluminescence", *Adv. Phys.* **33**, 595-660.

Table 1: Velocity exponents (dimensionless) relating to noise and luminescence (after van der Meulen, 1986 b)

Type of flow	Angle of attack, α	n (noise)	m (luminescence)
(i) Bubble	2°	0.9	–1.8
2° (no Xe)	0.7	—	
(ii) Sheet	4°	5.9	7.2
(iii) Sheet-cloud	7°	5.1	6.5
(iv) Vortex-cloud	11°	4.8	3.9

Table 2

C_{ref}/m/s	σ	α/°	Count for SGC CIPS
19.9	0.81	2.5	11.5
19.9 ~ 20	0.74	2.5	61
20.3	0.62	2.5	106.8
24.9	0.80	2.5	206.1
24.9 ~ 25	0.74	2.5	393.1
24.8	0.70	2.5	721.4
29.9	0.80	2.5	687.0
29.9 ~ 30	0.75	2.5	1298.6
29.7	0.71	2.5	1713.9

Background count per second: 45, 7, ← for error bar
Total trace length = 262 ns
Sampling frequency = 2 MHz for all.

Table 3 angle = 4°, σ *constant* (~ 1.1)

C_{ref}	Col. (i) Total no. photons	Col. (ii) Modal occupancy	Col. (iii) Number of windows	Col. (iv) Highest value of low frequency in Hz	Col. (v) Minimum value of high frequency in Hz
18.3	118,000	15 ± 5	7867	37.5 ± 13	750 ± 250
20.0	175,000	28 ± 5	6250	30 ± 5	1400 ± 250
22.0	215,000	40 ± 5	5375	26 ± 4	2000 ± 250
24.6	245,000	53 ± 5	4623	22 ± 2	2650 ± 250
25.8	260,000	62 ± 7	4194	20 ± 2	3100 ± 350
28.0	280,000	72 ± 7	3888	18.5 ± 2	3600 ± 350
30.0	280,000	74 ± 3 85 ± 3	-	-	-
32.1	310,000	92 ± 10	3370	16 ± 4	4600 ± 500

Table 4 C_{ref} *constant at 30 m/s; angle constant at* 4°, σ *varies*

σ	Col. (i) Total no. photons	Col. (ii) Modal occupancy	Col. (iii) Number of windows	Col. (iv) Highest value of low frequency in Hz	Col. (v) Minimum value of high frequency in Hz
0.9	295,000	-	-	-	-
1.0	290,000	-	-	-	-
1.1	289,000	-	-	-	-
1.2	288,000	72 ± 5	3512	17 ± 2	3600 ± 300
1.3	285,000	67 ± 6	4254	20 ± 2	3350 ± 300
1.4	267,000	63 ± 6	4238	20 ± 2	3150 ± 300
1.5	235,000	46 ± 7	5109	24 ± 4	2300 ± 350

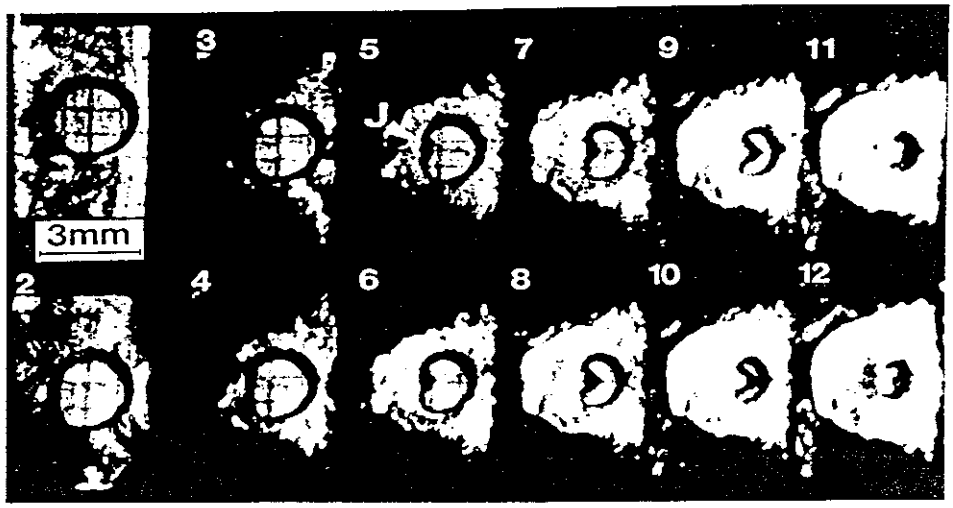

Figure 1

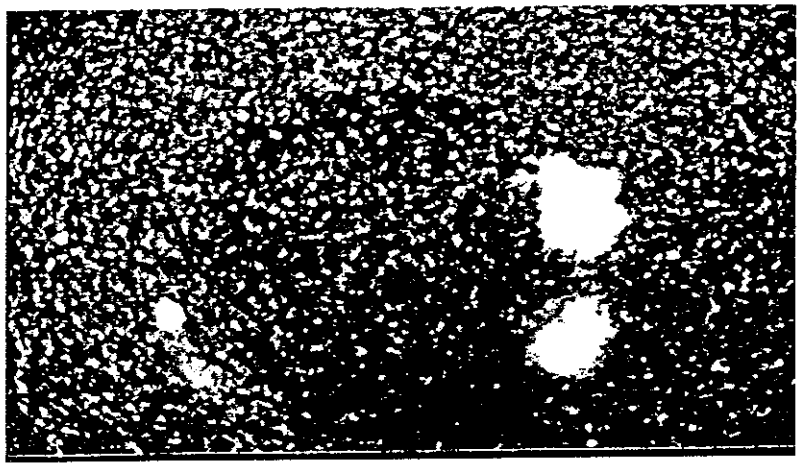

Figure 2

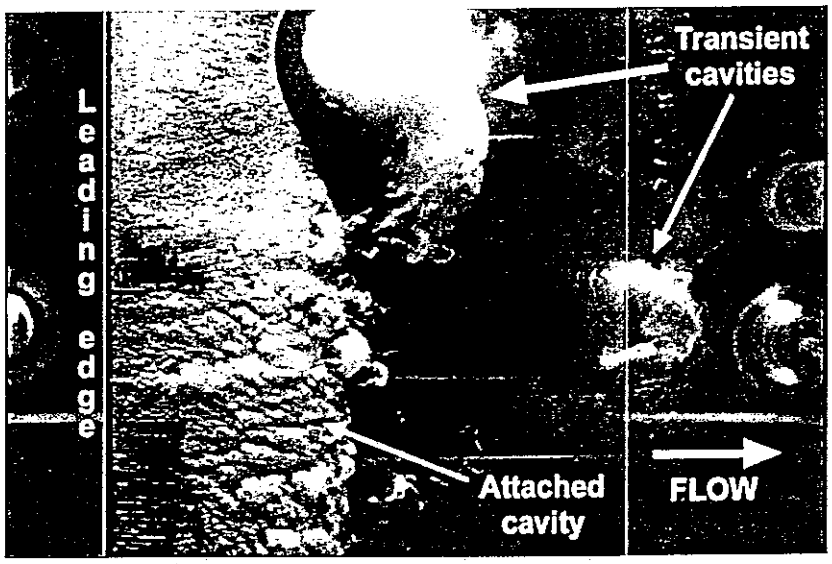

Figure 3

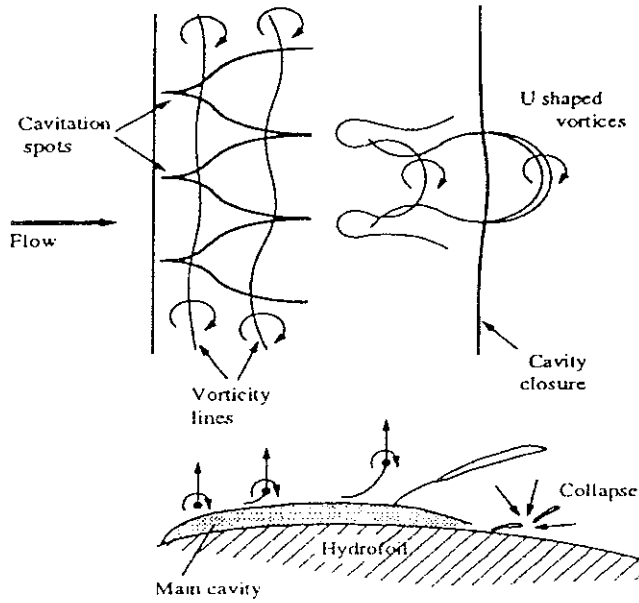

Figure 4

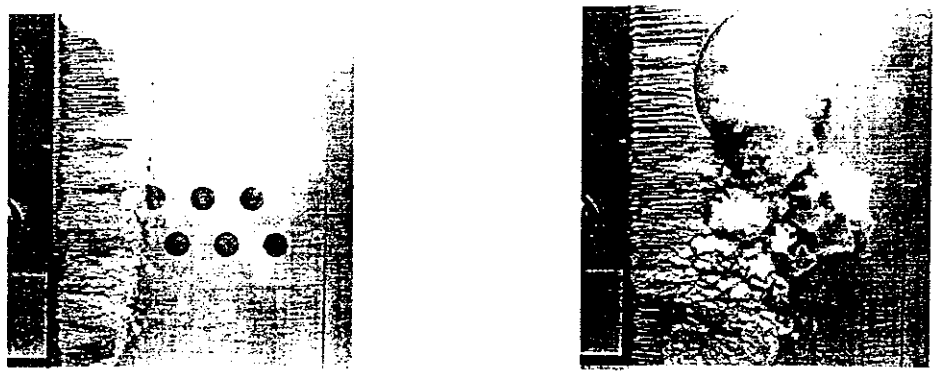

Figure 5

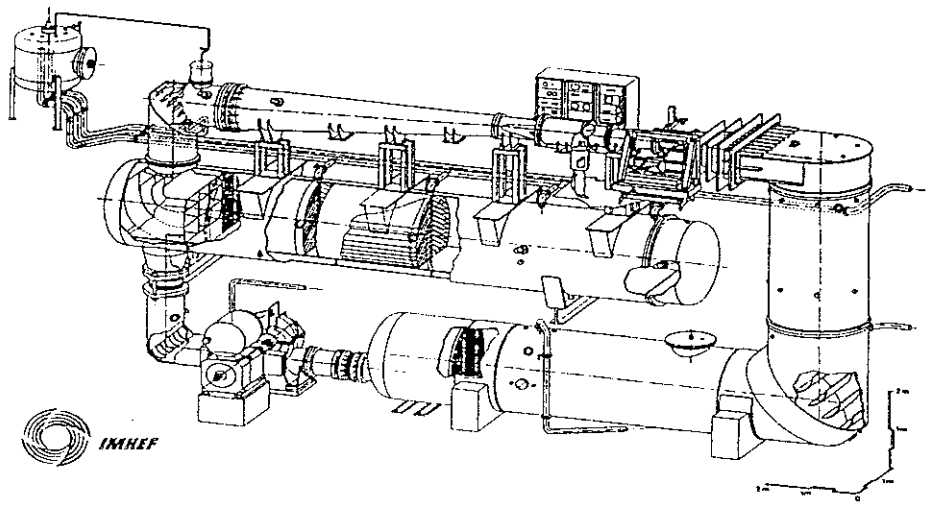

Figure 6

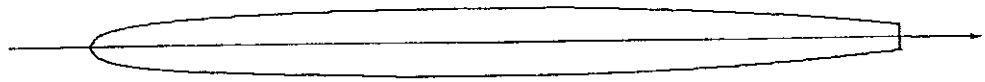

Figure 7

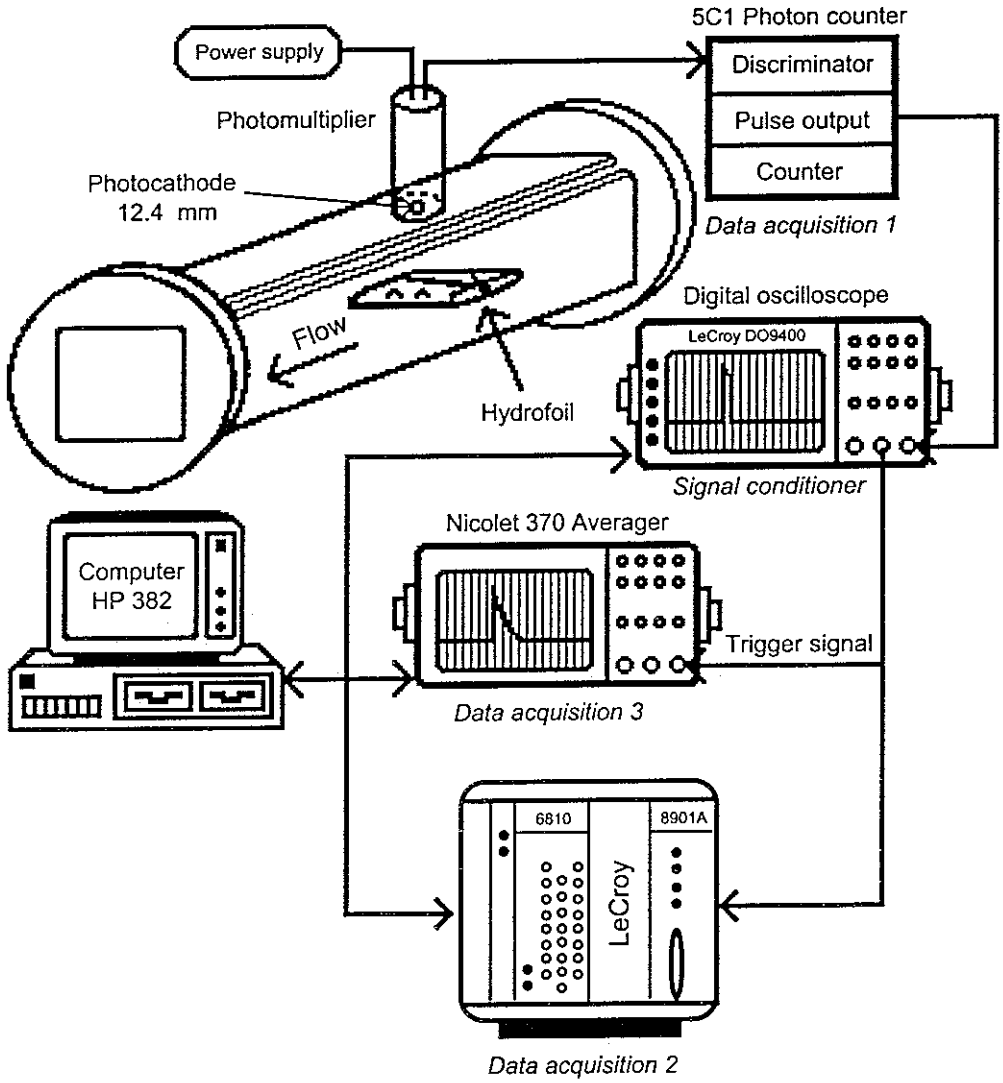

Figure 8

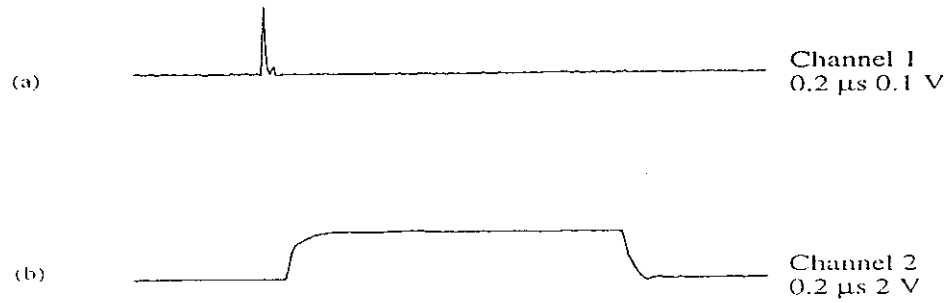

Figure 9

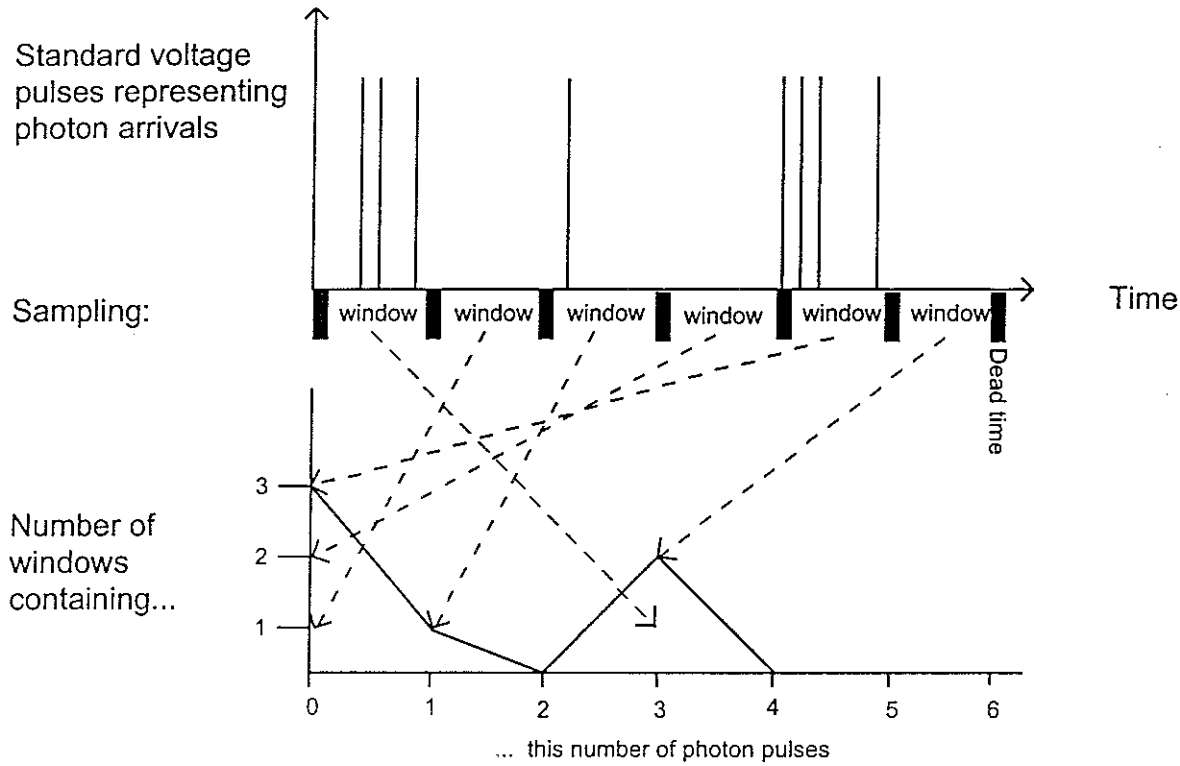
Standard voltage pulses representing photon arrivals
Sampling:
window
window
window
window
window
window
Dead time
Time
Number of windows containing...
3
2
1
0
1
2
3
4
5
6
... this number of photon pulses

Figure 10

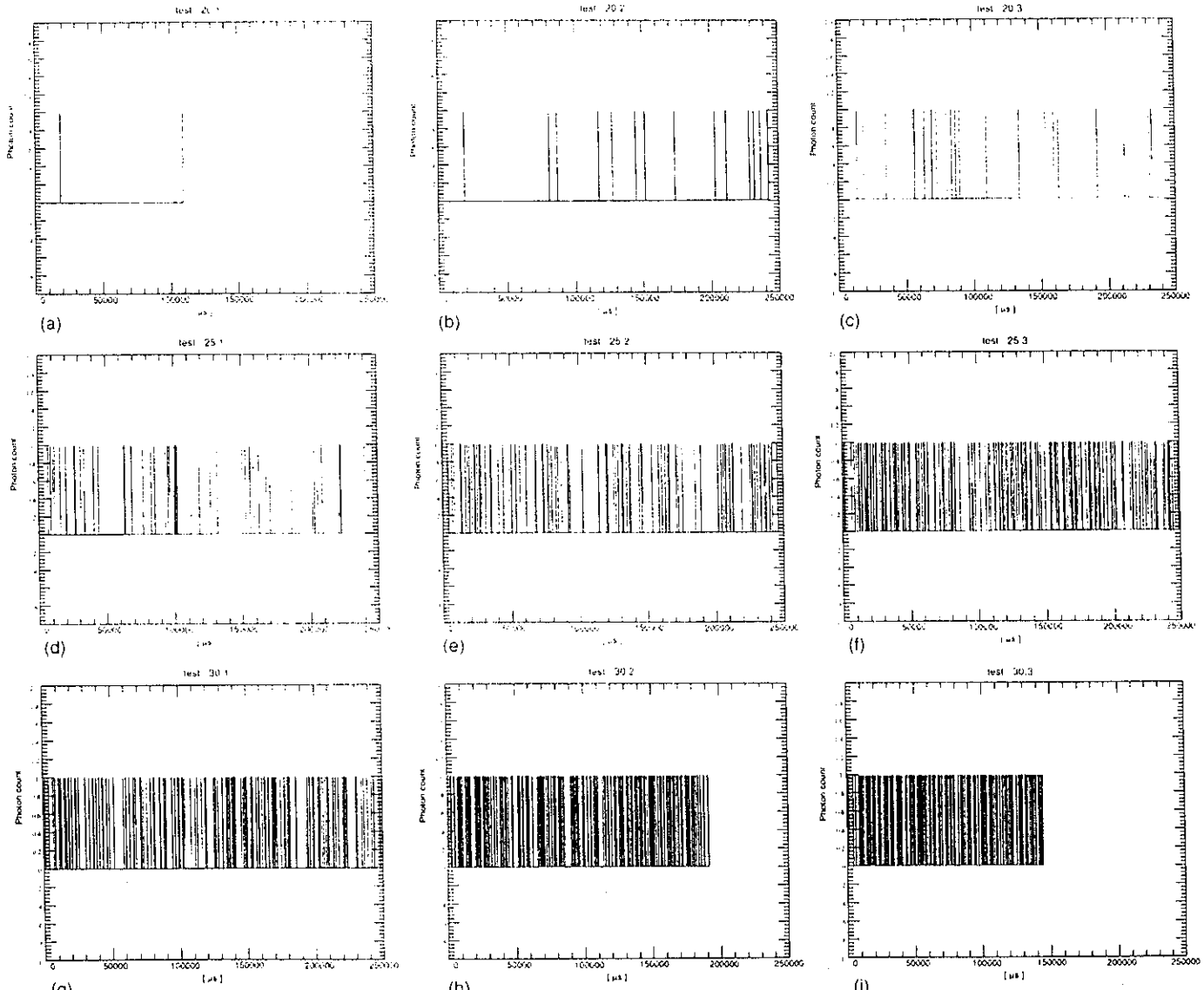

Figure 11

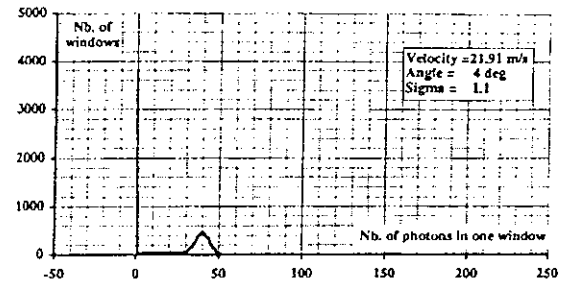

(a)

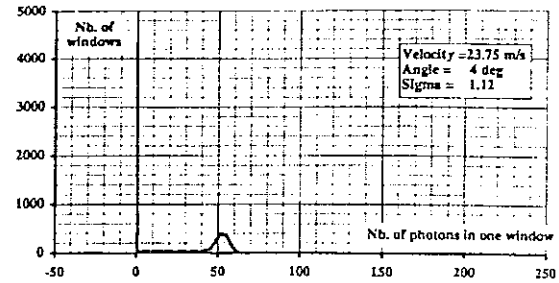

(b)

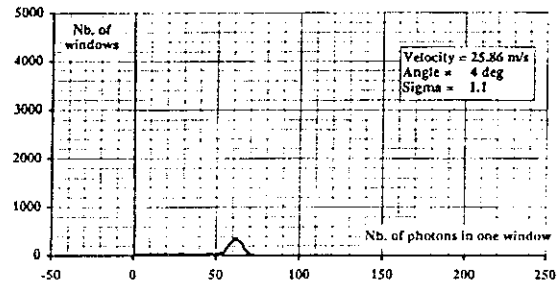

(c)

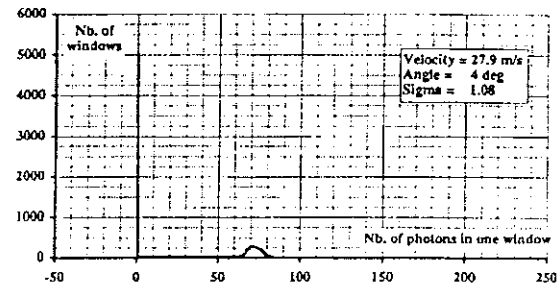

(d)

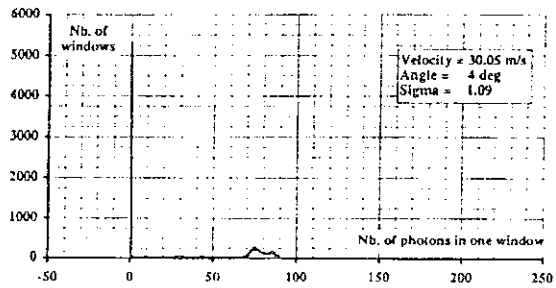

(e)

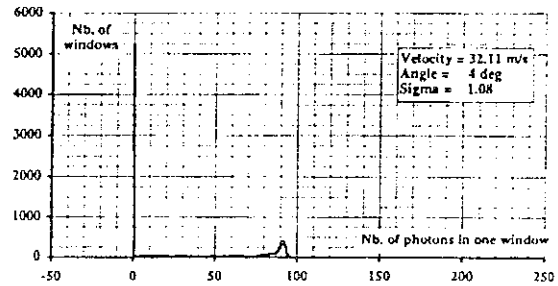

(f)

Figure 12

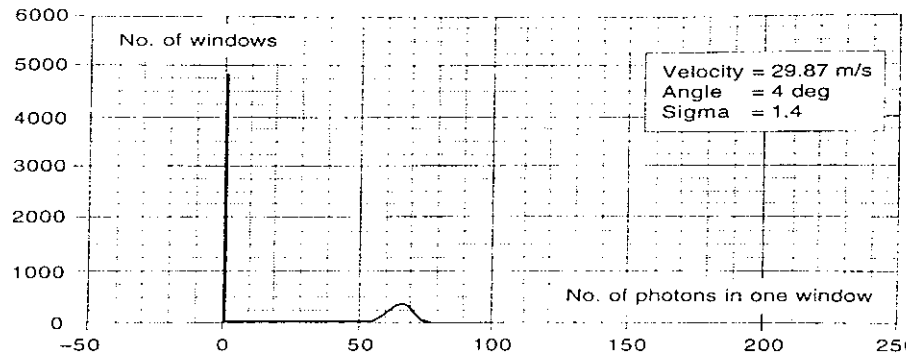
6000
5000
4000
3000
2000
1000
0
No. of windows
Velocity = 29.87 m/s
Angle = 4 deg
Sigma = 1.4
No. of photons in one window
-50
0
50
100
150
200
250

(c)

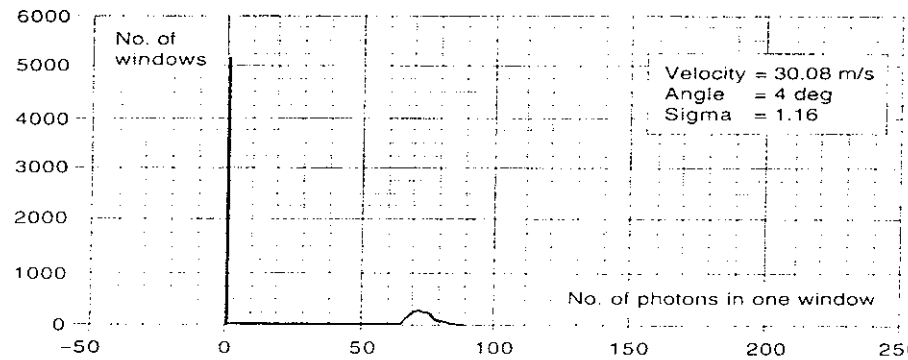
6000
5000
4000
3000
2000
1000
0
No. of windows
Velocity = 30.08 m/s
Angle = 4 deg
Sigma = 1.16
No. of photons in one window
-50
0
50
100
150
200
250

(d)

Figure 13

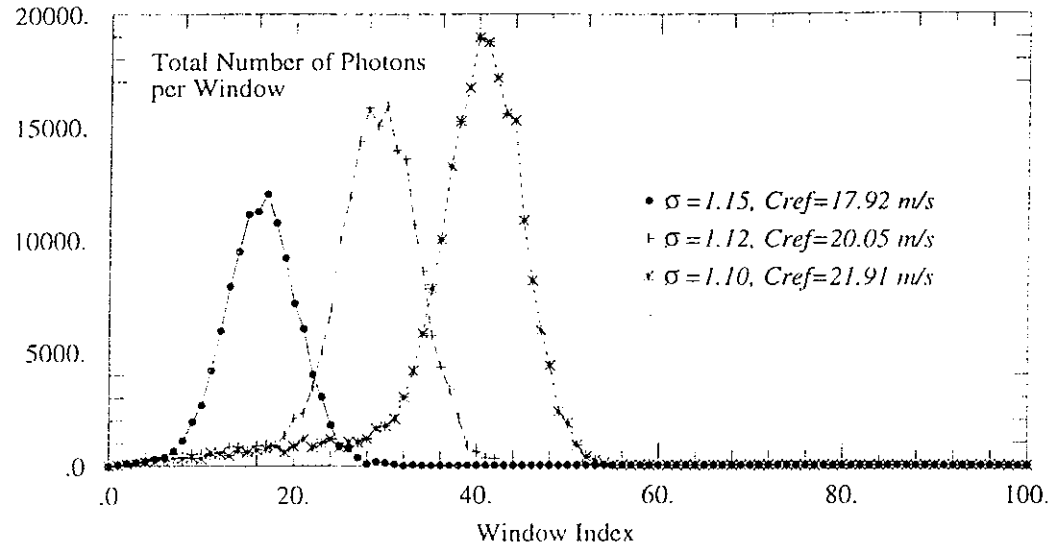
Total Number of Photons
per Window
σ = 1.15, Cref=17.92 m/s
σ = 1.12, Cref=20.05 m/s
σ = 1.10, Cref=21.91 m/s
20000.
15000.
10000.
5000.
.0
.0
20.
40.
60.
80.
100.
Window Index

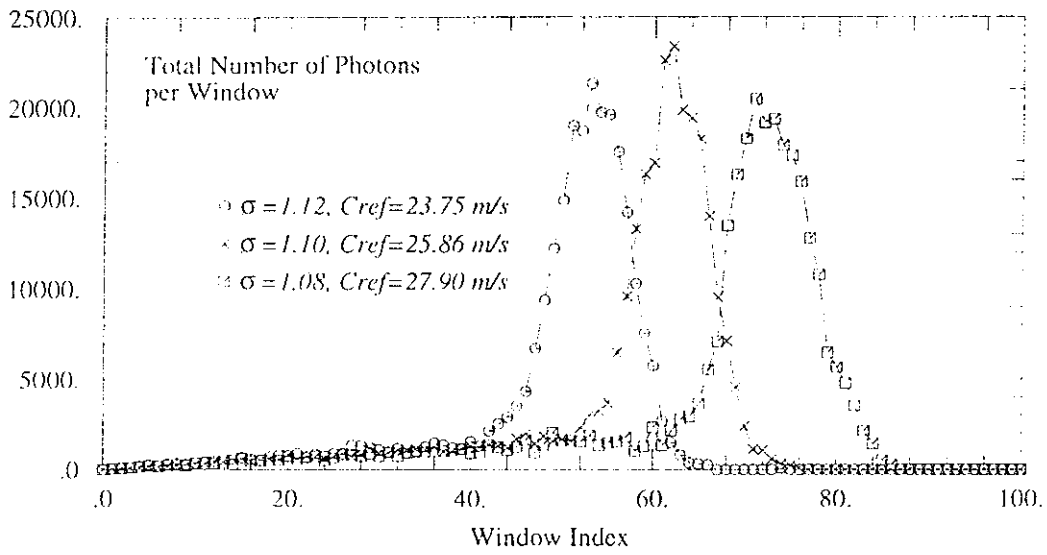
Total Number of Photons
per Window
σ = 1.12, Cref=23.75 m/s
σ = 1.10, Cref=25.86 m/s
σ = 1.08, Cref=27.90 m/s
25000.
20000.
15000.
10000.
5000.
.0
.0
20.
40.
60.
80.
100.
Window Index

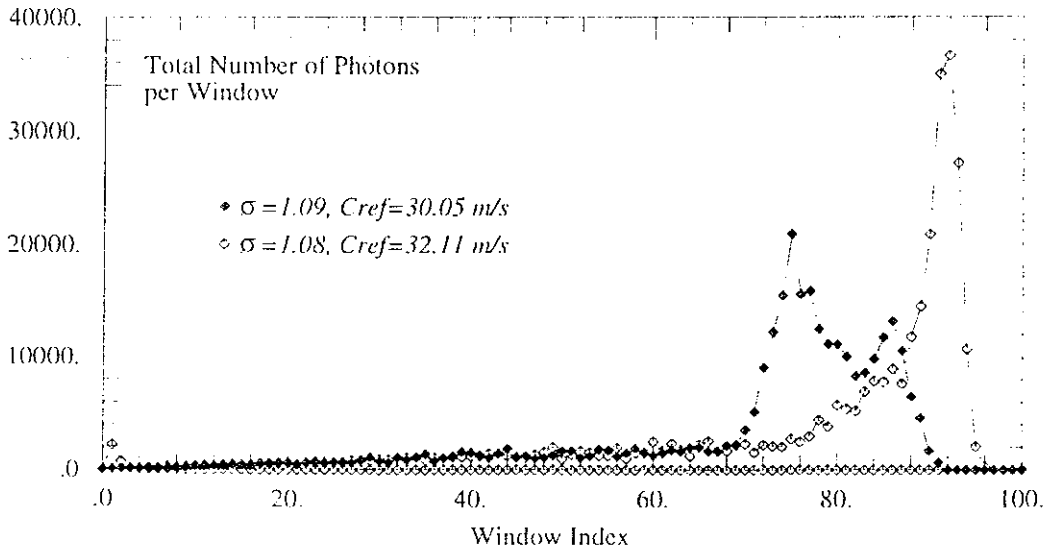
Total Number of Photons
per Window
σ = 1.09, Cref=30.05 m/s
σ = 1.08, Cref=32.11 m/s
40000.
30000.
20000.
10000.
.0
.0
20.
40.
60.
80.
100.
Window Index

Figure 14

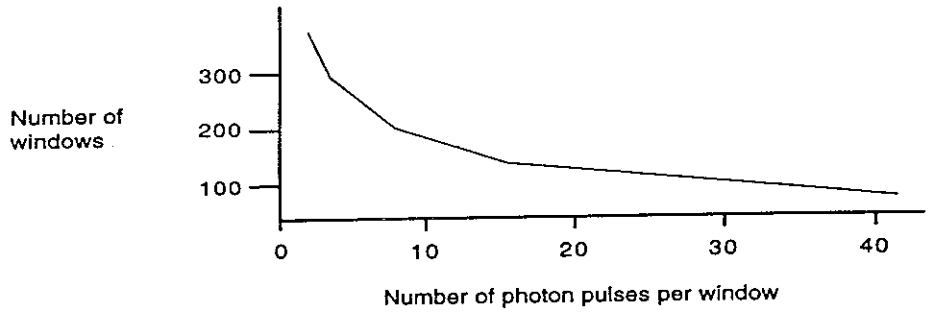

Figure 17

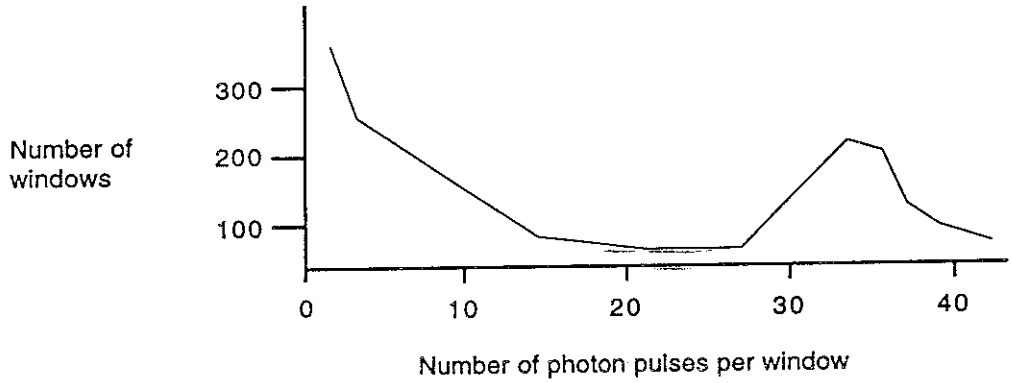

Figure 18